The distribution of methylated sulfur compounds, DMS and DMSP, in

Canadian Subarctic and Arctic marine waters during summer, 2015

Tereza Jarníková [1], John Dacey[2], Martine Lizotte[3], Maurice Levasseur [3]

and Philippe Tortell[1,4,5]

(1) Department of Earth, Ocean and Atmospheric Sciences, University of British Columbia, 2022 Main Mall, Vancouver BC, Canada V6T 1Z3

(2) Woods Hole Oceanographic Institution, Woods Hole, MA 02543.

(3) Université Laval, Department of Biology (Québec-Océan), Québec City, Québec, Canada.

(4) Department of Botany, University of British Columbia, 6270 University Blvd., Vancouver BC, Canada V6T 1Z4

(5) Peter Wall Institute for Advanced Studies, University of British Columbia, 6330 Crescent Blvd., Vancouver BC, Canada V6T 1Z4

Correspondence to: Tereza Jarníková (tjarniko@eoas.ubc.ca)

16   **Abstract**

17   **We present seawater concentrations of dimethylsulfide (DMS), and**

18   **dimethylsulfoniopropionate (DMSP) measured across a transect from the Labrador**

19   **Sea to the Canadian Arctic Archipelago, during summer 2015. Using an automated**

20   **ship-board gas chromatography system, and a membrane-inlet mass spectrometer,**

21   **we measured a wide range of DMS (~1 nM to 18nM) and DMSP (~1 nM to 150 nM)**

22   **concentrations. The highest DMS and DMSP concentrations occurred in a localized**

23   **region of Baffin Bay, where surface waters were characterized by high chlorophyll *a***

24   **(chl *a*) fluorescence, indicative of elevated phytoplankton biomass. Across the full**

25   **sampling transect, there were only weak relationships between DMS/P, chl *a***

26   **fluorescence and other measured variables, including positive relationships between**

27   **DMSP:chl *a* ratios and several taxonomic marker pigments, and elevated DMS/P**

28   **concentrations in partially ice-covered areas. Our high spatial resolution**

29   **measurements allowed us to examine DMS variability over small scales (<1 km),**

30   **documenting strong DMS concentration gradients across surface hydrographic**

31   **frontal features. Our new observations fill in an important observational gap in the**

32   **Arctic Ocean, and provide additional information on sea-air DMS fluxes from this**

33   **ocean region.   in this study constitute a significant contribution to the existing**

34   **Arctic DMS/P dataset, and provide a baseline for future measurements in the region.**

1. Introduction

The trace gas dimethylsulfide (DMS), a degradation product of the algal metabolite dimethylsulfoniopropionate (DMSP), is the largest natural source of sulfur to the atmosphere, accounting for over 90% of global biogenic sulfur emissions (Simó, 2001). Atmospheric DMS is rapidly oxidized to sulfate aerosols that act as cloud condensation nuclei (CCN), backscattering incoming radiation, increasing the albedo of low-altitude clouds and potentially cooling the Earth (Charlson et al., 1987). The seminal CLAW hypothesis proposed by Charlson et al. (1987) suggests that this negative radiative forcing will have cascading effects on marine primary productivity, leading to a DMS-mediated climate feedback loop. Although more recent work has disputed the mechanism of this biologically-mediated climate feedback (Quinn and Bates, 2011), the CLAW hypothesis has provided motivation for the widespread measurement of DMS in the global ocean over the past thirty years.

Beyond their potential role in regional climate forcing, DMS and DMSP also play critical ecological roles in marine microbial metabolism and food-web dynamics (for a complete overview; see Stefels et al., 2007). DMSP is believed to serve numerous physiological functions in phytoplankton, with suggested roles as an osmolyte, an anti-oxidant, and a cryoprotectant under different environmental conditions. Sunda et al. (2002) suggested that oxidative stressors, such as high solar radiation or iron limitation, may stimulate DMSP production in certain phytoplankton species. The production of this molecule is largely species-dependent, and can vary by three orders of magnitude among phytoplankton groups, with the highest intracellular concentrations typically reported in

57   dinoflagellates and haptophytes, and lower concentrations in diatoms (Keller, 1989).

58   After synthesis, DMSP can be cleaved to DMS and acrylate within algal cells, or

59   by heterotrophic bacteria acting on the dissolved DMSP ($DMSP_d$) pool in the water

60   column (Zubkov et al., 2001). The release of DMSP into the water column is believed to

61   be enhanced in physiologically stressed or senescent phytoplankton (Malin et al., 1998),

62   and can be stimulated by zooplankton grazing and viral lysis (Evans et al.,r 2007).

63   Bacteria can also utilize $DMSP_d$ as a sulfur source for protein synthesis (Kiene et al.,

64   2000), but this pathway does not lead to DMS release. The DMS yield of bacterial

65   DMSP metabolism (i.e. the fraction of consumed DMSP that is converted to DMS) varies

66   significantly, and may be influenced by the relative supply and demand of reduced sulfur

67   and carbon for bacterial growth (Kiene and Linn, 2000).

68   In environments with low anthropogenic aerosol concentrations, understanding

69   the impact of natural aerosol sources on cloud formation is critical to correctly estimating

70   climate forcing (Carslaw et al, 2013). Modeling studies have suggested that DMS

71   emissions could exert a particularly significant influence on CCN formation and regional

72   climate in polar regions, due to the low background concentrations of atmospheric

73   aerosols at high latitudes (Woodhouse et al., 2010) The effect of aerosol emissions on

74   cloud formation remains subject to some debate, with a modelling study (Browse et al

75   2014) suggesting only weak CCN response to Arctic organic aerosol flux. Nevertheless,

76   direct observations have demonstrated a link between sea surface DMS emissions and

77   particle formation events in the Arctic atmosphere (Chang et al., 2011; Mungall et al.,

78   2016), motivating further quantification of marine DMS emissions in Arctic regions.

79   To date, logistical constraints have limited the measurements of surface water

80   properties in many high latitude regions, and these areas remain relatively sparsely

81   sampled for DMS/P concentrations. Indeed, of the approximately 50,000 data points in

82   the global Pacific Marine Environmental Laboratory (PMEL) database of oceanic DMS

83   measurements (http://saga.pmel.noaa.gov/dms/), only 5% have been made in either Arctic

84   or Antarctic waters (~ 1600 and 1000 data points, respectively). Despite the relatively

85   limited sulfur observations in high latitude waters, an examination of the available data

86   reveals large differences in the water column DMS distributions of the Arctic and

87   Antarctic regions. While the summertime mean DMS concentration in the Arctic Ocean is

88   3.0 nM (close to the global mean value of 4.2 nM, derived from the PMEL data), the

89   mean summertime DMS concentration in the Southern Ocean is ~ 3 times higher at 9.3

90   nM. Moreover, several areas of extraordinarily high DMS concentrations (>100 nM) have

91   been observed in various regions of the Southern Ocean (DiTullio et al. 2000; Tortell et

92   al. 2011), whereas no study to date has observed DMS concentrations above 25 nM in

93   Arctic waters. The available data thus suggest contrasting dynamics of DMS/P

94   production in the two polar regions (i.e. Arctic vs. Antarctic).

95   Although Arctic and Antarctic regions share several key physical characteristics,

96   most notably strong seasonal cycles in sea ice cover and solar irradiance, there are some

97   critical differences. Much of the pelagic Southern Ocean is an iron-limited, High

98   Nutrient Low Chlorophyll (HNLC) regime, with large seasonal changes in mixed layer

99   depths (MLD) (Boyd et al., 2001). Low iron conditions, and seasonally-variable mixed

100   layer light levels may induce oxidative stress (particularly in ice-influenced stratified

101   waters) and thus promote high DMS production (Sunda et al., 2002). In addition, parts of

102   the Southern Ocean are characterized by extremely high biomass of *Phaeocystis*

103   *antarctica* (Smith et al., 2000), a colonial haptophyte that is a prodigious producer of

104   DMSP and DMS (Stefels et al., 2007). By comparison, the salinity-stratified surface

105   waters of the Arctic Ocean are believed to be primarily limited by macronutrient (i.e.

106   nitrate) availability (Tremblay et al., 2006), with a maximum phytoplankton biomass that

107   is at least an order of magnitude lower than that observed in the Southern Ocean (Carr et

108   al., 2006). Despite the relatively low phytoplankton biomass over much of the Arctic

109   Ocean, reasonably high summertime DMS levels (max ~ 25 nM) have been observed in

110   some regions. It is also important to note that significant Arctic phytoplankton biomass

111   and primary productivity may occur in sub-surface layers (Martin et al. 2010), and in

112   under-ice blooms (Arrigo et al., 2012). The quantitative significance of these blooms for

113   DMS production is unknown at present (Galindo et al., 2014).

114   Quantifying the spatial and temporal distribution of DMS and DMSP in the Arctic

115   Ocean is particularly important in light of the rapidly changing hydrographic conditions

116   across this region. Rapid Arctic warming over the past several decades has been

117   associated with a significant reduction in summer sea ice extent, resulting in higher

118   mixed layer irradiance levels and a longer phytoplankton growing season (Arrigo et al.,

119   2008). Arrigo et al (2008) suggested that continued warming and sea-ice loss could lead

120   to a three-fold increase in primary productivity over the coming decades. The effects of

121   these potential changes on DMS/P concentrations and cycling remain unknown, but it has

122   been suggested that future changes in Arctic Ocean DMS emissions could modulate

123   regional climatic patterns (Levasseur, 2013). Indeed, modeling work has suggested that

124   cooling associated with increased DMS production and emissions in less ice-covered

125   polar regions may help offset warming associated with loss of sea-ice albedo (Gabric et

126   al., 2004; Cameron-Smith et al., 2011) The important climatic and biological roles of

127   reduced sulfur compounds, combined with altered marine conditions under a warming

128   environment, provide the motivation for a deeper understanding of the distribution and

129   cycling of DMS and related compounds in Arctic waters.

130   In this article, we present a new data set of DMS and DMSP concentrations in

131   Arctic and Subarctic waters adjacent to the Canadian continental shelf. We used a

132   number of recent and emerging methodological approaches to measure these compounds

133   in a continuous ship-board fashion. In particular, we used membrane inlet mass

134   spectrometry (MIMS) to measure DMS with extremely high spatial resolution (i.e. sub-

135   km scale), and the recently developed organic sulfur sequential chemical analysis robot

136   (OSSCAR), for automated analysis of DMS and DMSP. Our goal was to utilize the

137   sampling capacities of the MIMS and OSSCAR systems to make simultaneous

138   measurements of DMS/P in Subarctic Atlantic and Arctic waters, in order to expand the

139   spatial coverage of the existing DMS/P dataset, and identify environmental conditions

140   leading to spatial variability in the concentrations of these compounds.

141   **2. Methods**

142   **2.1 Study Area**

143   Our field study was carried out on board the *CCGS Amundsen* during Leg 2 of the 2015

144   GEOTRACES expedition to the Canadian Arctic, from July10 to August 20, 2015. We

145   sampled along a ~ 10,000 km transect from Quebec City, Quebec, to Kugluktuk,

146   Nunavut. Data collection commenced off the coast of Newfoundland, and included

147   waters of the Labrador Sea, Baffin Bay and the Canadian Arctic Archipelago (Figure 1).

148   The cruise transect covered two main distinct geographic domains – the Baffin

149   Bay/Labrador Sea region, and the Canadian Arctic Archipelago (CAA). The majority of

150   the surface water in the CAA is from Pacific-sourced water masses, as a shallow sill near

151   Resolute restricts the westward flow of Atlantic-sourced water (Michel et al., 2006). Flow

152   paths through the CAA are complex. The region is characterized by a network of shallow,

153   narrow straits that are subject to significant regional variability in local mixing and tidal

154   processes, and strongly influenced by riverine input, which drives stratification (Carmack

155   et al, 2011). In contrast, both Atlantic- and Pacific-sourced waters mix in the Baffin Bay

156   and Labrador Sea regions, and this confluence drives a strong thermohaline front, leading

157   to lower stratification than in the CAA (Carmack et al, 2011).

158   **2.2 Underway sampling systems**

159   We utilized two complementary underway sampling systems to measure reduced

160   sulfur compounds; MIMS (Tortell, 2005), and OSSCAR (Asher et al., 2015). Detailed

161   methodological descriptions of these systems have been published elsewhere ((Tortell,

162   2005, 2011), (Asher et al., 2015), and only a brief overview is given here.

163   **2.2.1 OSSCAR**

164   The OSSCAR instrument consists of an automated liquid handling / wet

165   chemistry module that is interfaced to a custom-built purge-and-trap gas chromatograph

166   (GC) equipped with a pulsed flame photometric detector (PFPD) for sulfur analysis. A

167   custom LabVIEW program is used to automate all aspects of the sample handling and

168   data acquisition. During analysis, unfiltered seawater (3 - 5 ml) from an underway supply

169   (nominal sampling depth ~ 5 m) is drawn via automated syringe pump into a sparging

170   chamber. DMS is then stripped out of solution (4 minutes of 50 ml min^{-1} N$_2$ flow) onto a

171   1/8" stainless steel trap packed with carbopack at room temperature. Rapid electrical

172   heating of the trap (to ~260°C), causes DMS desorption onto a capillary column (Restek

173   SS MXT, 15m, 80 °C, 2 ml min^{-1} N$_2$ flow) prior to detection by the PFPD (OI Analytical,

174   Model 5380). Light emitted during combustion in the PFPD is converted to a voltage and

175   recorded by a custom built Labview data acquisition interface. Following the completion

176   of DMS analysis, 5 N sodium hydroxide is added to the sparging chamber for 14 minutes

177   to cleave DMSP in solution to DMS, following the method of Dacey and Blough (Dacey

178   and Blough, 1987). The resulting DMS is sparged out of solution and measured as

179   described above. The sparging chamber is then thoroughly rinsed with Milli-Q water,

180   and the process can be repeated. As we used unfiltered seawater for our analysis, it is

181   important to note that we measured total DMSP (DMSP$_t$) concentrations, which represent

182   the sum of dissolved and particulate pools.

183   We measured an in-line standard (20 nM) every 4-5 samples (at most every 3

184   hours) to ensure that the system was functioning correctly, and to correct for potential

185   detector drift. The mean standard error of daily point standards was 0.55 nM, and we

186   consider this to represent the precision of our emerging method (significant efforts are

187   underway to increase this precision). To correct the underway data for instrument drift,

188   point standard measurements were smoothed with a 3-pt running mean filter, interpolated

189 to the time-points of sample measurements, and compared to the known standard

190 concentration to provide a drift correction factor for every seawater data point. Six-point

191 calibration curves were performed every two days, using DMS standards (ranging from 0

192 to 18nM), produced from automated dilutions of a primary DMS stock and Milli-Q water

193 (see Asher et al., 2015). The limit of detection of the system was calculated from the

194 calibration curve using the formula $C_{LOD} = 3s_{y/x} \div b$, where C_{LOD} is the concentration limit

195 of detection, $s_{y/x}$ is the standard error of the regression , and b is the slope of the

196 regression line. With this approach, we derived a mean limit of detection of 1.4 nM. The

197 mean linear calibration curve R^2 value, taken over all calibration curves, was 0.9887.

198   The OSSCAR system is designed to automate the collection of seawater for

199 sequential analysis of DMS, DMSO, and DMSP in a single sample. During our cruise,

200 however, we experienced problems with the DMSO reductase enzyme used to convert

201 DMSO to DMS for analysis, and we therefore configured the instrument to run only

202 DMS and DMSP at sea, with one cycle requiring roughly 30 minutes. We experienced

203 general technical difficulties with the instrument during the early phases of the cruise,

204 and no OSSCAR data are thus available for the first half of the transect.

205 **2.2.2 MIMS**

206 We used MIMS to obtain very high frequency measurements (~ several data points per

207 minute) of DMS concentrations and other gases in surface seawater. Using this system,

208 seawater from the ship's underway loop was pumped through a flow-through sampling

209 cuvette, attached, via a silicone membrane, to a quadrupole mass spectrometer (Hiden

210 Analytical HPR-40). DMS was measured by detecting ions with a mass to charge ratio of

211   62 (m/z 62) every ~30 seconds. To achieve constant sample temperature prior to contact

212   with the membrane, seawater was passed through a 20 foot coil of stainless steel tubing

213   immersed in water bath held at 4 °C (Tortell et al. 2011). The system pressure (as

214   measured by the Penning Gauge) remained stable during operation ($\sim$1.3 – 1.5 x 10^{-6}

215   Torr). The DMS signal was calibrated using liquid standards that were produced by

216   equilibrating 0.2 μm filtered seawater with a constant supply of DMS (m/z 62) from a

217   calibrated permeation device (VICI Metronics). The primary effluent from the

218   permeation tube (held at 30 ± 0.1 °C in a custom-built oven) was split among several

219   capillary outflows and mixed into a N_2 stream controlled at 50 ml min^{-1} using a pressure

220   regulator and fixed length / diameter tubing. This system enabled us to achieve a range

221   of DMS / N_2 mixing ratios that were bubbled into standard bottles held in an incubator

222   tank supplied with continuously flowing seawater. Concentrations of DMS in the

223   standard bottles were cross-validated by measuring discrete samples using the OSSCAR

224   system. The limit of reliable detection of the MIMS is $\sim$ 2nM (Tortell 2005).

225   **2.3 Post-processing of DMS data**

226   Raw data outputs (voltages) for both OSSCAR and MIMS measurements were processed

227   into final concentrations using MATLAB scripts. For OSSCAR data, raw voltages were

228   captured with a sampling frequency of 5 Hz. Sulfur peaks eluting off the GC column

229   were integrated using a custom MATLAB script, with correction for baseline signal

230   intensities.   DMS concentrations were derived from peak areas using the calibration

231   curves as described above.

232   **2.4 Ancillary seawater data**

233   Shipboard salinity, temperature, wind speed, and chlorophyll *a* (chl *a*)

234   fluorescence measurements were collected using several underway instruments. We used

235   a Seabird Electronics thermosalinograph (SBE 45) for continuous surface temperature

236   and salinity measurements, and a Wetlabs Fluorometer (WetStar) to measure chl *a*

237   fluorescence, as a proxy for phytoplankton biomass. We note that the chl *a* fluorescence

238   data are subject to significant diel cycles associated with light-dependent fluorescence

239   quenching. All sensors were calibrated prior to and following the summer expedition.

240   Conductivity Temperature Depth (CTD) profiles were used to measure vertical profiles of

241   salinity and potential temperature at 17 stations, from which we computed density using

242   the Seawater Toolbox in MATLAB. The mixed layer depth (MLD) was defined as the

243   depth where density exceeded surface values by 0.125 kg m^{-3}. Sea ice concentrations

244   were obtained from the AMSR-E satellite product (Cavelieri et al. 2006) with a spatial

245   resolution of 12.5 km. The percent ice cover along the cruise track was derived from a

246   two dimensional interpolation of the ship's position in time and space against the daily

247   sea ice data.

248   All correlation analyses (Pearson's *r*) were computed in MATLAB, using the

249   corrcoef function. Sample sizes were as follows: 33,250 data points in the MIMS DMS

250   dataset, 344 in the OSSCAR DMS dataset, and 318 in the OSSCAR DMSP dataset.

251   **2.5 Phytoplankton biomass and taxonomic composition**

252   In addition to underway data, samples for the quantification of photosynthetic and

253   accessory pigments (Table 1) were collected at a number of discrete oceanographic

254   stations (see Table 2). For each station, duplicate samples (250-500 mL) for chl *a* analysis

255   were filtered onto pre-combusted 25 mm glass fiber filters (Whatman GF/F) using low

256   vacuum pressure (<100 mm Hg). Filters were stored at -20 ºC and chl *a* was determined

257   within a few days of sample collection using fluorimetric analysis following the method

258   of Welschmeyer (Welschmeyer 1994). Duplicate 1-2 L samples were filtered onto pre-

259   combusted 25 mm GF/F for pigment analysis by reverse-phase High-Performance Liquid

260   Chromatography (HPLC). Filters were dried with absorbent paper, flash frozen in liquid

261   nitrogen and stored at -80 ºC until analysis following the method of Pinckney et al

262   (1994). We used several diagnostic pigments as markers for individual phytoplankton

263   groups, as described by Coupel et al (2015) (see Table 1). Following HPLC pigment

264   processing, data were interpreted with the chemotaxonomy program CHEMTAX V1.95,

265   using the pigment ratio matrix described by Taylor et al (2013).

266   **2.6 DMS Sea-Air Flux**

267   We derived sea-air fluxes of DMS from MIMS measurements of DMS

268   concentrations, as these data had higher resolution and spatial coverage than OSSCAR

269   observations. We computed sea-air flux as:

270            $$F_{DMS} = k_{DMS} (DMS_{SW}) (1 - A)^{0.4} \tag{1}$$

271   where DMS_{sw} is the concentration of DMS in the surface ocean (surface atmospheric

272   DMS is assumed to be zero) and k_{DMS} is the gas transfer velocity derived from the

273   equations of Nightingale et al. (2000), normalized to the temperature and salinity-

274   dependent DMS Schmidt number of Saltzman et al. (1993). The term A represents the

275   proportion of sea ice cover, and the scaling exponent of 0.4 accounts for the effects of sea

276   ice on gas exchange and is derived from the laboratory work of Loose et al. (2009). (We

277   note that this scaling does not capture all processes present in sea-ice dominated regimes,

278   such as turbulence generated by sea ice melt.) Sea surface salinity and temperature

279   measurements described in section 2.5 were used in the calculations. Wind speed data

280   were obtained from the ship's anemometer (AAVOS data, Environment Canada),

281   corrected to a height of 10 m above the sea surface.

282   **3. Results**

283   **3.1 Oceanographic setting**

284   Figures 1 and 2 show the distribution of hydrographic properties across our cruise

285   survey region. Over our sampling area, surface water temperatures varied between -1.2

286   and 10.2 °C, while surface salinity ranged from 10.7 to 34.7 psu (Figure 1). The warmest

287   and most saline waters were found in the Labrador Sea, with cold fresher waters in

288   Hudson Strait and the Canadian Arctic Archipelago. Underway chl *a* fluorescence varied

289   between 0.04 and 2.96 µg L^{-1}, averaging 0.20 µg L^{-1}. The highest chl *a* fluorescence was

290   observed in a localized region within Baffin Bay, in the vicinity of a sharp temperature

291   and salinity frontal zone (Figure 1). Mixed layer depth (MLD) ranged from ~ 5 - 50 m,

292   and were deepest in the Labrador Sea and shallowest in the stations of the Canadian

293   Arctic Archipelago. Sea ice cover was variable across the survey transect, with ice-free

294   waters in the Labrador Sea, and significant ice cover in the northern Hudson Bay and

295   parts of the Canadian Arctic Archipelago (Figure 2).

296   **3.2 Phytoplankton biomass and taxonomic distributions**

297   Using measurements of accessory photosynthetic pigments, we examined spatial patterns

298   in the taxonomic composition of phytoplankton assemblages (see Table 1 for a

299   description of HPLC marker pigments and their associated phytoplankton taxa).The

300   distribution of pigments across our sampling stations is presented in Table 2, along with

301   measurements of mixed layer depth and ice cover, while CHEMTAX-derived assemblage

302   estimates are shown in Table 3. In order to remove large potential differences in total

303   phytoplankton biomass, we normalized pigment concentrations to total chl a

304   concentrations measured using HPLC (see Methods, section 2.5).

305   CHEMTAX pigment analysis shows that all stations in the study area were diatom-

306   dominated, although haptophyte, dinoflagellate, and prasinophyte markers were detected

307   in varying quantities at all stations (see Table 3). Total HPLC-measured chl *a* was

308   relatively low throughout the study area, ranging from 0.11 to 0.56 μg L^{-1}.

309   **3.3 Observed DMS/P concentration ranges**

310   The DMS data shown in Figure 1 are derived from MIMS measurements, since

311   these have wider geographic coverage and greater spatial resolution than OSSCAR data.

312   DMS concentrations measured with MIMS ranged from 0.2 nM to 12 nM, averaging 2.7

313   (± 1.5) nM. The highest values were observed in the northern Labrador Sea, Baffin Bay

314   and Hudson Strait, with lower values through much of the Arctic Archipelago.

315   Figure 3 shows the distribution of DMS, measured by both MIMS and OSSCAR,

316   along the cruise track. DMS concentrations measured with OSSCAR ranged from 0.1 to

317   18 nM, averaging 3.2± 2.4 nM. As described in the discussion,22% of our derived DMS

318   concentrations fell below the limit of detection. In general, we observed reasonably good

319   coherence between DMS measurements made by our two analytical systems, with similar

320   absolute values of data and spatial patterns. There were, however, notable offsets in the

321 early August measurements (~ km 7000 cruise track, Figure 3a), when OSSCAR DMS

322 data were consistently higher than MIMS data. Notwithstanding this offset (for which

323 potential reasons are addressed in the discussion), the coherent spatial patterns in data

324 derived from these independent methods is encouraging, particularly given the rather low

325 precision of our current OSSCAR system.

326   The spatial distribution of DMSP concentrations (measured with OSSCAR) along

327 the cruise track is also shown in Figure 3. Concentrations ranged from <1 nM to 160 nM,

328 and averaged 30 ± 29 nM. DMSP:chl *a* ratios measured from HPLC chl a data ranged

329 from 52.31 nmol μg^{-1} to 181.4nmol μg^{-1}. Examination of the data in Figure 3

330 reveals that high DMS concentrations were sometimes, but not always, accompanied by

331 high DMSP concentrations. For example, a sharp increase in measured DMSP

332 concentrations (around 7000-7400 km) on the cruise track was accompanied by a sharp

333 increase in DMS measured by both instruments, while low-DMS waters observed around

334 km 9400 along the transect also showed very little DMSP. Over the portion of the

335 transect where measurements of both DMS and DMSP were available, the OSSCAR-

336 measured concentrations of these compounds exhibited a statistically significant positive

337 correlation ($r = 0.52$, $p < 0.001$). There were, however, a number of regions where

338 increased DMS concentrations were not accompanied by increases in DMSP (e.g. ~ km

339 10,000).

340 **3.4 Sea-Air Flux**

341 Figure 4 shows DMS sea-air fluxes as computed from MIMS-measured DMS seawater

342 concentrations, wind speed and sea ice cover. DMS sea-air fluxes ranged from < 1 to 80

343   μmol S m^{-2} day^{-1}, with peak sea-air flux calculated around km 5500 on the cruise track.

344   Sea-air flux is highly dependent on wind speed and sea ice cover, with the result that even

345   high concentrations of seawater DMS yielded low sea-air flux when low wind and/or

346   high sea ice was present (e.g. km 2100, 7200, 8300). Conversely, very high sea-air fluxes

347   were observed when moderately high DMS concentrations coincided with high wind

348   speeds and ice-free waters (e.g. km 5400).

349   **3.5 Comparison of gradients in DMS data with hydrographic features**

350   The high sampling frequency of MIMS measurements allows the comparison of

351   DMS observations with other underway environmental variables, and enables the

352   quantification of small-scale DMS concentration gradients in near real-time. Figure 2

353   shows a cruise track record of MIMS-measured DMS concentrations in relation to

354   salinity, temperature, chl *a* fluorescence, and ice cover. Several sharp increases in DMS at

355   around kms 2100, 3300, and 3800 along the cruise track were accompanied by strong

356   gradients in temperature and, to a lesser extent, salinity (Figure 2). These regions

357   correspond to areas in the Labrador Sea and Baffin Bay. An increase in DMS

358   concentrations in Baffin Bay around km 7200 in the cruise track (Figure 2a) was

359   associated with a simultaneous drop in sea-surface temperature and salinity, in close

360   proximity to a sharp increase in chl *a* fluorescence along the cruise track (Figure 2c) (see

361   Figure 1). As shown in Figure 3b, this localized region exhibited the highest

362   concentrations of DMSP along the transect. Interestingly, this area was also characterized

363   by strong gradients in sea ice concentrations, and the low salinity waters are indicative of

364   localized ice melt. Figures 1d and 2d also show the large-scale salinity gradients in the

365   Hudson Bay and the Canadian Arctic Archipelago, highlighting the freshwater influx in

366   these near-shore areas. In contrast to our observations in Baffin Bay, DMS

367   concentrations showed relatively little variability across these salinity gradients.

368   In order to more closely examine small-scale variability in DMS and other surface

369   water variables, we calculated spatial gradients in the data to examine the coherence of

370   frontal features in DMS, salinity, temperature and chl *a* fluorescence. For this analysis,

371   we computed gradients in each oceanographic variable within a neighborhood of 100

372   points surrounding each point. Gradients (G) for each variable (DMS, SST, chl *a*, and

373   salinity) were calculated at each point x as follows:

374    $$G_x = \frac{V_{x+50} - V_{x-50}}{D_{x+50} - D_{x-50}} \quad (2)$$

375   Here, G is gradient (in units of change per km), V is the value of the variable at a

376   point, x, and D is the cruise track distance at x. A neighborhood of 100 points,

377   corresponding to a distance of ~25 km, was subjectively chosen because it best captured

378   the observed variability in the data, representing an intermediate value between a

379   localized neighborhood (e.g. 10 points), which would only consider changes close to the

380   point, and a large neighborhood (e.g. 1000 points), which would smooth the features. The

381   results of this analysis (Figure 5) qualitatively demonstrate a coherence of DMS gradients

382   with salinity, chlorophyll, and sea surface temperature.

383   **3.6 Correlation with ancillary oceanographic variables**

384   We computed Pearson correlation coefficients of DMS and DMSP with underway

385   measurements of salinity, sea surface temperature, chl *a* fluorescence, and sea ice cover.

386   We also examined the potential relationships between DMS concentrations and MIMS-

387   derived $p\text{CO}_2$, and $\Delta\text{O}_2/\text{Ar}$ (Tortell et al., in preparation). The results can be seen in Table

388   4. Only correlations significant at the 0.05 level are included. Only weak correlations are

389   seen between MIMS-measured DMS data and ancillary variables, and OSSCAR DMS

390   data did not exhibit any significant correlations with any ancillary variables, including

391   measured of phytoplankton taxonomic distributions. A significant positive correlation (r

392     $= 0.66$, $p<0.001$) was found between DMSP and underway chl a fluorescence. Over the

393   whole transect, we observed a weak negative correlation between DMS/P and sea-ice

394   cover ($r = -0.26$ for DMS, and $r=-0.34$ for DMSP, $p< 0.001$ in both cases). A weak

395   positive correlation was found between DMSP/chl a and ice cover ($r = 0.52$, $p< 0.04$),

396   suggesting potential roles for sea-ice microalgae in DMSP production at the sampled

397   stations. It is interesting to note that elevated chl a fluorescence and DMSP

398   concentrations often occurred in areas of intermediate ice cover (km 3300, 7300 and 9200

399   along the cruise track), potentially reflecting the influence of ice-edge blooms or under-

400   ice phytoplankton assemblages. Potential mechanisms for these features are addressed in

401   the discussion.

402   **4. Discussion**

403   Our results provide a new dataset of reduced sulfur compounds in an under-

404   sampled region of the Arctic Ocean, enabling an examination of DMS/P variability in

405   relation to various oceanographic properties on a range of spatial scales. Below, we focus

406   our discussion on the observed relationship between gradients in DMS and other

407   oceanographic variables, and discuss the comparability of the two DMS measurement

408   methods utilized.   We compare our results to previously published measurements in the

409   Arctic, situating our results in the context of the changing hydrography and

410   phytoplankton ecology of the Arctic Ocean.

411   **4.1 Comparability of MIMS and OSSCAR measurements**

412   The OSSCAR and MIMS instruments have previously shown good agreement in

413   measured DMS concentrations in the Subarctic Pacific Ocean (Asher et al. 2015).

414   Similarly, we observed relatively good coherence between the two methods (Figure 3)

415   over much of our cruise track. The largest exception to this occurred around km 7000,

416   when DMS measurements measured by OSSCAR were significantly higher than those

417   measured by MIMS. This region was characterized by very high DMSP measurements

418   (often one order of magnitude higher than the DMS measurements). If small amounts of

419   DMS remained in the OSSCAR system after DMSP analysis, sample carry-over could

420   contribute to higher measured concentrations in the subsequent DMS analysis. In order

421   to minimize this potential artifact, the system was thoroughly rinsed with MilliQ water

422   after every run. The effectiveness of this rinse was tested by subsequently purging DMSP

423   standards without NaOH, and no carryover was observed. It is possible, however, that

424   this approach was not entirely efficient. Another potential cause of the higher OSSCAR

425   DMS measurements may be due to cell breakage during the sparging process in

426   OSSCAR. In this scenario, there is the potential for release of intracellular DMSP and

427   DMSP lyase into solution, which would lead to artificially high measured DMS

428   concentrations. It is not possible for us to quantify the magnitude of such a potential

429   artefact, but we note that its magnitude would likely depend on the taxonomic

430   composition of phytoplankton assemblages. Wolfe et al (2002) showed that sample

431 sparging led to an increase in DMS production by both the haptophyte *Emiliana huxleii*

432 and the dinoflagellate *Alexandrium*. Unfortunately, due to limited coverage of discrete

433 sampling, we do not have any estimates of phytoplankton community composition in the

434 region where MIMS and OSSCAR showed the greatest discrepancies. Notwithstanding

435 these potential caveats, we suggest that the two methods show strong promise to provide

436 complementary information on DMS/P (and DMSO) concentrations in surface ocean

437 waters.

438   One challenge going forward is to increase the reproducibility and sensitivity of

439 OSSCAR measurements, and this is an area of active work in our group. The version of

440 our system used in 2015 had a detection limit of roughly 1.4 nM, and was thus far less

441 sensitive than many conventional GC methods, which can achieve sub-nM detection

442 limits. Our detection limit was of only minor consequence for DMSP measurements,

443 given that 72% of measured DMSP concentrations were higher than 10 nM, and less than

444 3% fell below 1.4 nM. The relatively low sensitivity was somewhat more problematic

445 for DMS, with approximately 22% of our OSSCAR-measured DMS values below 1.4

446 nM. Nonetheless, as discussed below, we believe that the OSSCAR data, in combination

447 with our MIMS data, provide useful information on the spatial distribution of both DMSP

448 and DMS in Arctic waters.

449 **4.2 Towards a regional Arctic data base of DMS/P concentrations**

450   Figure 6 shows a comparison between our Arctic DMS measurements (made by

451 OSSCAR) and other summertime Arctic DMS data in the PMEL database. For this

452 comparison, only PMEL measurements made above the Arctic circle (66.56° N) in June-

453   August are included, resulting in a total of 415 data points. As shown in Figure 6, the

454   majority of available summertime PMEL DMS/P measurements are found in the Atlantic

455   region of the Arctic, and in the Bering Sea, with limited data in the Canadian Archipelago

456   (for an overview of Arctic DMS/P studies performed to date, see Levasseur, 2013). For

457   the sake of visual clarity, the presentation of data in Figure 6a is based on DMS

458   measurements made by OSSCAR, whereas both sets of data were included in the

459   frequency distribution analysis (Figure 6b). The results presented in Figure 6 suggest that

460   our measurements are representative of the broader Arctic context, with generally similar

461   data frequency distributions (Figure 6b) for all three DMS datasets (MIMS, OSSCAR,

462   and PMEL). From the map, we see that the spatial footprint of our measurements

463   complement the existing summer data, helping to expand the spatial coverage of DMS

464   observations in the Arctic Ocean.

465   In addition to complementing the existing PMEL DMS database, our new

466   observations also build on a number of other reduced sulfur measurements in the

467   Canadian Sector of the Arctic Ocean. Observations of DMS and DMSP derived from

468   several past Arctic and subarctic Atlantic surveys are summarized in Table 5. This table

469   focuses mainly on DMS and DMSP measurements made in the Canadian sector and

470   Greenland waters, serving to provide context for our measurements performed in similar

471   environments. The data presented in Table 5 are obtained from different times of year,

472   and from phytoplankton assemblages of varying taxonomic composition, allowing us to

473   examine DMS and DMSP concentrations in surface waters under a range of

474   environmental and ecological conditions.   For example, Bouillon et al. (2002) observed

475   low DMS concentrations (<1nM) during a large spring diatom bloom (~ 15 μg L^{-1}chl a)

476   in the North Water region. In contrast, higher DMS concentrations have been reported

477   later in the season when total phytoplankton biomass is lower, and taxonomic

478   composition has shifted away from diatom-dominance. Working in the same geographic

479   region as Bouillon, Motard-Côté et al. (2012) reported higher late summer (September)

480   DMS levels (maximum = 4.8nM), which were accompanied by moderate chl a

481   concentrations (0.2-1 μgL^{-1}), while Luce et al. (2011) reported very low DMS (<1nM)

482   associated with moderate chl a concentrations (0.2-2 μgL^{-1}) in a flagellate dominated

483   community in late fall (October-November), with DMS decreasing towards the later

484   months. A similar pattern was observed in the northwest subarctic Atlantic by Lizotte et

485   al. (2012), who associated elevated reduced sulphur (DMSP) production with flagellate

486   and prymnesiophyte communities in midsummer and fall, in contrast to early-season

487   diatom blooms with little associated DMSP and DMS. This seasonal decrease in DMS

488   levels may be potentially attributable to light limited primary productivity, and

489   diminishing capacity for light-induced oxidative stress, which has been shown to increase

490   DMS/P production (Sunda et al., 2002).

491   To date, the highest recorded Arctic water column measurements of DMS (25nM)

492   and DMSP (160 nM) have been observed during mid-summer blooms of the haptophyte

493   *Phaeocystis* at the ice edge (see Matrai and Vernet, 1997; Gali and Simo, 2010). Our mid-

494   season (July-August) study of similar areas shows moderately high DMS (up to 18 nM)

495   accompanied by relatively low chl a (0.11- 1.06 μgL^{-1}) in a mixed community where

496   flagellates and prasinophytes are present.

497   Together, the available data (Table 5 and our measurements) are consistent with a

498   seasonal cycle in Arctic and subarctic reduced sulfur distributions. Early season diatom-

499   dominated blooms exhibit high biomass and primary productivity but low DMS/P

500   accumulation, while mid-summer phytoplankton assemblages dominated by haptophytes

501   and dinoflagellates display lower phytoplankton biomass but higher reduced sulfur

502   accumulation. This pattern is similar to the summertime 'DMS paradox' reported in a

503   number of temperate and sub-tropical waters (Simo and Pedrós-Alió, 1999). In the fall,

504   both Arctic primary productivity and DMS/P production decrease with the onset of lower

505   temperatures and increased ice cover. Our data are consistent with this general scenario,

506   representing a mixed-species assemblage with moderate biomass and DMS/P

507   accumulation.

508   **4.3 Gradients in DMS and hydrographic frontal structures**

509   The high resolution afforded by the MIMS dataset allows for the observation of

510   fine-scale variability in DMS concentrations at the sub-kilometer scale. Previous studies

511   (Tortell, 2005; Tortell et al., 2011) have quantified fine-scale variability in DMS

512   concentrations, demonstrating de-correlation length scales on the order of 10s of Km, and

513   often shorter than that of other oceanographic variables such as temperature and salinity.

514   These length-scales provide information on the spatial scale of processes driving the

515   majority of variability in DMS concentrations. Figures 2 and 5 clearly demonstrate that

516   gradients in DMS and chl *a* fluorescence often co-occur with strong gradients in

517   temperature and salinity. This suggests a potential role for hydrographic fronts in driving

518   changes in DMS concentrations. Several potential mechanisms may explain this

519 phenomenon. For example, the frontal mixing of distinct water masses, driven by

520 currents, wind, or melting ice, may introduce nutrients into a low-nutrient water column,

521 stimulating localized primary productivity (Tremblay et al. (2011) and potentially

522 increasing DMS/P production. Note that this localized increase in productivity and

523 potential DMS/P production would operate independently of the overall seasonal

524 progression towards increased DMS/P production during the latter summer growth

525 season. Mixing of water masses may also potentially expose water column phytoplankton

526 to light shock or osmotic stress by mixing them upwards in the water column or

527 introducing an abrupt salinity gradient. Both of these factors could contribute to elevated

528 DMSP production, given its hypothesized role as an intracellular osmolyte and anti-

529 oxidant (Stefels et al., 2007). Although our data do not allow mechanistic interpretation

530 for the underlying causes of DMS variability in surface waters, the high resolution

531 afforded by MIMS measurements enables real-time observations of DMS gradients,

532 which may be useful in the design of future process studies examining the driving forces

533 for elevated DMS accumulation.

534

535 **4.4 Influence of phytoplankton assemblage composition and mixed layer depth**

536 Previous work has addressed the role of phytoplankton taxonomic composition

537 and irradiance levels (Stefels et al, 2007) in driving the cycling of DMS/P in marine

538 waters. Here we discuss the potential influence of these factors across our survey region.

539 The majority of the sampled stations were characterized by very shallow mixed layer

540 depths (MLD; Table 2) resulting from strong salinity-based stratification of surface

541   waters. Light stress associated with shallow MLD may contribute to elevated DMSP : chl

542   *a* ratios, and previous studies (Vallina 2007) have shown high correlation between solar

543   irradiance and surface DMS concentrations. In our dataset, however, there was no

544   overall correlation between MLD and DMSP : Chl ratios. We did, however, observe

545   elevated DMSP concentrations at two stations (BB3 and CAA6) with shallow MLDs.

546   The elevated DMSP : chl *a* ratios measured in our study may also reflect the

547   presence of high-DMSP producing taxa, a phenomenon previously reported by other

548   groups (Matrai et al., 1997; Gali et al., 2010; Lizotte et al., 2012). When comparing our

549   DMSP: chl *a* ratios to other measurements, it is important to note that we measured

550     $DMSP_t$, while many other groups present $DMSP_p$, without taking into account the

551   dissolved fraction ($DMSP_d$). As the dissolved DMSP pool typically makes up a small

552   (though highly variable) portion of the total water column DMSP pool, the use of DMSPt

553   does not likely have a large effect on derived DMSP:chl a ratios (Kiene et al., 2000;

554   2006). Despite the potential caveats raised above, the $DMSP_t$:chl *a* ratios we measured

555   across our sampling stations (52-182 nmol μg^{-1}) were broadly similar to $DMSP_p$:chl *a*

556   values found by Motard-Côté et al. (15-229 nmol μg^{-1}) in the same region in September

557   (Motard-Côté et al., 2011). In contrast, our measured $DMSP_t$:chl *a* ratios are significantly

558   higher than those measured by Luce et al. (maximum of 39 nmol μg^{-1}) (Luce et al., 2007)

559   and Matrai and Vernet (maximum 17 nmol μg^{-1}) at diatom-dominated stations in the

560   Barents Sea (Matrai and Vernet., 1997). The higher DMSP : Chl ratios we measured may

561   be attributable to the presence of mixed (rather than diatom-dominated) assemblages

562   present in the study area at the time of sampling. We cannot, however, draw any firm

563 conclusions on the role of taxonomy in controlling DMSP:Chla, as we were unable to

564 detect any significant correlations between DMSP:chl *a* and HPLC pigment markers for

565 different phytoplankton groups.

566   To conclude, our observations do not permit us to establish a firm link between

567 MLD, phytoplankton taxonomy and DMS/P concentrations. Other factors, including

568 bacterial activity and zooplankton grazing are potential contributing factors, but we lack

569 the data needed to examine the importance of these processes.

570   **4.5The interaction of DMS/P and sea ice**

571   The presence of sea ice exerts a strong control on polar phytoplankton by

572 controlling irradiance levels in the water column (Levasseur 2013), and influencing

573 vertical mixing, stratification and nutrient accumulation. It is thus expected that the

574 presence of sea-ice may affect DMS/P cycling. In a 2010 study, Gali et al (2010) found

575 that Arctic sea ice melt drove stratification of nutrient rich surface water, triggering a

576 sharp increase in primary productivity, with associated elevated DMS and DMSP levels.

577 These authors also showed that experimental exposure of phytoplankton to high light

578 conditions (mimicking those that would follow the breakup of sea ice) led to near-total

579 release of intracellular DMSP, providing one possible explanation for elevated DMSP

580 levels in the water column. A number of studies also show that the ice, itself, can be a

581 potentially significant reservoir of reduced sulfur, associated with bottom ice-algae

582 (Levasseur et al (1994).

583   The weak negative correlation we observed between sea ice cover and DMS/P

584 concentration is consistent with the idea that sea ice cover limits insolation, thereby

585   reducing primary productivity and DMS/P production. In general, the drivers of DMSP

586   and DMS production differ – though DMSP production has been shown to be directly

587   influenced by sea ice melt in under-ice blooms (Galindo et al., 2014), the production of

588   DMS from DMSP is largely dependent on the metabolism of in situ bacterial assemblages

589   (Evans et al, 2007), and may therefore be uncoupled from the influence of ice on

590   phytoplankton activity. It is interesting to note, however, that several sharp increases in

591   DMS (observed with MIMS) occurred simultaneously with the occurrence of small

592   amounts of sea ice (<20% total cover) (Figure 2, kms 3400 and 7200 on the cruise track).

593   Limited station data also indicate high DMSP:chl a ratios in areas with a comparatively

594   high sea ice cover, at stations BB3 and CAA6 (Table 2). At the time of our sampling,

595   both of these stations were characterized by very low phytoplankton biomass (0.11 μg L^{-1}

596   and 0.20 μg L^{-1}chl a, respectively) and had particularly high DMSP: chl a ratios (129

597   nmol μg^{-1} and 182 nmol μg^{-1}, respectively). This suggests a potential role for ice-edge

598   effects, either through the melt-induced stimulation of reduced sulfur production in

599   DMSP rich phytoplankton taxa, or through the release of ice-associated DMSP into the

600   water column. Figures 2d and 2e show decreased salinity in partially ice-covered areas

601   (e.g. around kms 4400, 7300, and 9200), suggesting some melt-water stratification

602   effects. Previous groups have also reported elevated DMS and DMSP concentrations in

603   partially ice-covered water and ice-edge regions in the Arctic Ocean (Matrai and Vernet

604   (1997),   Gali et al. (2010) and Leck and Persson (1997)).

605   =

606

5. Conclusion

We present a high spatial resolution dataset of reduced sulfur measurements through the Canadian sector of the Arctic Ocean and Subarctic Atlantic. We demonstrate the utility of high-resolution DMS measurements for comparison with other oceanographic variables, and show the coherence of DMS gradients with fine-scale surface hydrographic structure, suggesting elevated DMS production in some oceanographic frontal zones. We also observed elevated DMS/P values in partially ice-covered regions, suggesting that ice-edge effects may stimulate DMS/P production. Our data serve to significantly expand the existing spatial coverage of reduced sulfur measurements in the Arctic, providing a baseline for future studies in this rapidly changing marine environment. Future warming of surface waters and sea-ice melt could lead to increased concentrations and sea-air fluxes of DMS, though significantly more observations will be needed to substantiate this.

Acknowledgements: This work was supported by grants from the Natural Sciences and Engineering Research Council of Canada (NSERC) through the Climate Change and Atmospheric Research program (Arctic-GEOTRACES). We are grateful to the captain and crew of the *CCGS Amundsen* for their invaluable support in this work.

Data Availability:

All data are available at the following github repository:

https://github.com/tjarnikova/Jarnikova_Canadian_Arctic_DMS_supldata (DOI: 10.5281/zenodo.160225)

629   **References**

630   Arrigo, K.R., van Dijken, G., and Pabi, S.: Impact of a shrinking Arctic ice cover on

631   marine primary production, Geophys. Res. Lett., 35, L19603,

632   doi:10.1029/2008GL035028, 2008.

633

634   Arrigo, K.R., Perovich, D.K., Pickart, R.S., and Brown, Z.W.: Massive phytoplankton

635   blooms under Arctic sea ice, Science, 336,1408, doi:10.1126/science.1215065,

636   2012.

637

638   Asher, E., Dacey, J., Jarníková, T., and Tortell, P.: Measurement of DMS, DMSO, and

639   DMSP in natural waters by automated sequential chemical analysis, Limnol.

640   Oceanogr-Meth., 13, 451–462, doi:10.1002/lom3.10039, 2015.

641

642   Asher, E., Dacey, J., Stukel, M., Long, M.C., and Tortell, P.: Processes driving seasonal

643   variability in DMS, DMSP, and DMSO concentrations and turnover in coastal

644   Antarctic waters, Limnol. Oceanogr., 62, 104-124, doi: 10.1002/lno.10379, 2016.

645

646   Bouillon, R.C., Lee, P.A., de Mora, S.J., and Levasseur., M.: Vernal distribution of

647   dimethylsulphide, dimethylsulphoniopropionate, and dimethylsulphoxide in the

648   North Water in 1998, Deep-Sea Res., 49, 5171-5189, doi:10.1016/S0967-

649   0645(02)00184-4, 2002.

650

651   Boyd, P.W., Crossley, A.C., DiTullio, G.R., Griffiths, F.B., Hutchins, D.A., Queguiner,

652   B., Sedwick, P.N. and Trull, T.W.: Control of phytoplankton growth by iron supply

653   and irradiance in the subantarctic Southern Ocean: Experimental results from the

654   SAZ Project, J. Geophys. Res., 106, 31573–31583, doi:10.1029/2000JC000348,

655   2001.

656

657 Cameron-Smith, P., Elliott, S., Maltrud, M., Erickson, D., and Wingenter, O.: Changes in

658   dimethyl sulfide oceanic distribution due to climate change, Geophys. Res. Lett.,

659   38, L07704, doi:10.1029/2011GL047069.

660

661 Carmack, E., and McLaughlin, F.: Towards a recognition of physical and geochemical

662   change in Subarctic and Arctic Seas, Prog. Oceanogr., 90, 90-104, doi:

663   10.1016/j.pocean.2011.02.007, 2011.

664

665 Carr, M.-E., Friedrichs, M.A.M, Schmeltz, M., Aita, M.N., Antoine, D., Arrigo, K.R.,

666   Asanuma, I., Aumont, O., Barber, R., Behrenfeld, M. Bidigare, R., Buitenhuis,

667   E.T., Campbell, J., Ciotti, A., Dierssen, H., Dowell, M., Dunne, J., Esaias, W.,

668   Gentili, B., Gregg, W., Groom, S., Hoepffner, N., Ishizaka, J., Kameda, T., Le

669   Quéré, C., Lohrenz, S., Mara, J., Mélin, F., Moore, K., Morel, A., Reddy, T., Ryan,

670   J., Scardi, M., Smyth, T., Turpie, K., Tilstone, G., Waters, K., and Yamanaka, Y.: A

671   comparison of global estimates of marine primary production from ocean color,

672   Deep-Sea Res. Pt. II., 53, 741–770, doi:10.1016/j.dsr2.2006.01.028, 2006.

673

674 Cavelieri, D.J., Markus, T., Hall, D. K., Gasiewski, A. J., Klein, M., and Ivanoff, A.:

675   Assessment of EOS Aqua AMSR-E Arctic Sea Ice Concentrations Using Landsat-7

676   and Airborne Microwave Imagery, IEEE T. Geosci. Remote., 44, 3057-3069, doi:

677   10.1109/TGRS.2006.878445, 2006.

678

679 Chang, R., Sjostedt, S., Pierce, J., Papakyriakou, T., Scarratt, M., Michaud, S.,

680   Levasseur, M., Leaitch, R., and Abbatt, J.: Relating atmospheric and oceanic DMS

681   levels to particle nucleation events in the Canadian Arctic, J. Geophys. Res., 116,

682   D00S03, doi:10.1029/2011JD015926, 2011.

683

684 Charlson, R., Lovelock, J., Andreae, M., and Warren, S.: Oceanic phytoplankton,

685   atmospheric sulphur, cloud albedo and climate, Nature, 326, 655–661,

686   doi:10.1038/326655a0, 1987.

687

688 Coupel, P., Matsuoka, A., Ruiz-Pino, D., Gosselin, M., Marie, D., Tremblay, J.-É., and

689   Babin, M.: Pigment signatures of phytoplankton communities in the Beaufort Sea,

690   Biogeosciences, 12, 991–1006, doi:10.5194/bg-12-991-2015, 2015.

691

692 Dacey, J., and Blough, N.V.: Hydroxide decomposition of dimethylsulfoniopropionate to

693   form dimethylsulfide, Geophys. Res. Lett., 14, 1246-1249,

694   doi:10.1029/GL014i012p01246, 1987.

695

696 DiTullio, G., Grebmeier, J., Arrigo, K., Lizotte, M., Robinson, D., Leventer, A., Barry, J.,

697   VanWoert, M., and Dunbar, R.: Rapid and early export of Phaeocystis antarctica

698   blooms in the Ross Sea, Antarctica, Nature, 404, 595–598, doi:10.1038/35007061,

699   2000.

700 Evans, C., Kadner, S. V., Darroch, L.J., Wilson, W. H., Liss, P. S., and Malin, G.: The

701   relative significance of viral lysis and microtzooplankton grazing as pathways of

702   dimethylsulfoniopropionate (DMSP) cleavage: An Emiliana huxleyi culture study,

703   Limnol. Oceanogr., 52, 1036-1045, doi: 10.4319/lo.2007.52.3.1036, 2007.

704

705   Gabric, A., Simó, R., Cropp, R., Hirst, A., and Dachs, J.: Modeling estimates of the

706   global emission of dimethylsulfide under enhanced greenhouse conditions, Global

707   Biogeochem. Cy., 18, GB2014, doi:10.1029/2003GB002183, 2004.

708

709   Galí, M, and Simó, R.: Occurrence and cycling of dimethylated sulfur compounds in the

710   Arctic during summer receding of the ice edge, Mar. Chem., 122, 105-117,

711   doi:10.1016/j.marchem.2010.07.003, 2010.

712

713   Galindo, V., Levasseur, M., Mundy, C.J., Gosselin, M., Tremblay, J. -É., Scarratt, M.,

714   Gratton, Y., Papakiriakou, T., Poulin, M., and Lizotte, M.: Biological and physical

715   processes influencing sea ice, under‐ice algae, and dimethylsulfoniopropionate

716   during spring in the Canadian Arctic Archipelago, J. Geophys. Res-Oceans, 119,

717   3746–3766, doi:10.1002/2013jc00949, 2014.

718

719   Galindo, V., Levasseur, M., Mundy, C.J., Gosselin, M., Scarratt, M., Papakyriakou, T.,

720   Stefels, J., Gale, M., Tremblay, J.-É., and Lizotte, M.: Contrasted sensitivity of

721   DMSP production to high light exposure in two Arctic under-ice blooms, J. Exp.

722   Mar. Biol. Ecol., 475, 38–48, doi:10.1016/j.jembe.2015.11.009, 2016.

723

724   Keller, M.D.: Dimethyl sulfide production and marine phytoplankton: the importance of

725   species composition and cell size, Biol. Oceanogr., 6, 375-382,

726   doi:10.1080/01965581.1988.10749540, 1989.

727

728   Kiene, R., Linn, L. J., and Bruton, J.A.: New and important roles for DMSP in marine

729   microbial communities, J. Sea Res., 43, 209-224, doi: 10.1016/S1385-

730   1101(00)00023-X, 2000.

732   Kiene, R.P., and Linn, L.J.: Distribution and turnover of dissolved DMSP and its

733   relationship with bacterial production and dimethylsulfide in the Gulf of Mexico,

734   Limnol. Oceanogr., 45, 849-861, doi:10.4319/lo.2000.45.4.0849, 2000.

736   Kiene, R., and Slezak, D.: Low dissolved DMSP concentrations in seawater revealed by

737   small‐volume gravity filtration and dialysis sampling, Limnol. Oceanogr.-Meth., 4,

738   80–95, doi:10.4319/lom.2006.4.80, 2006.

740   Lana, A., Bell, T.G., Simó, R., Vallina, S.M., Ballabrera-Poy, J., Kettle, A.J., Dachs, J.,

741   Bopp, L., Saltzman, E.S., Stefels, J., Johnson, J.E., and Liss, P.S.: An updated

742   climatology of surface dimethlysulfide concentrations and emission fluxes in the

743   global ocean, Global Biogeochem. Cy., 25, GB1004, doi:10.1029/2010GB003850,

744   2011.

746   Leck, C., and Persson, C.: The central Arctic Ocean as a source of dimethyl sulfide

747   Seasonal variability in relation to biological activity, Tellus B, 48B(2), 156–177,

748   doi:10.1034/j.1600-0889.1996.t01-1-00003.x, 1996.

750   Levasseur, M., Gosselin, M., and Michaud, S.: A new source of dimethylsulfide (DMS)

751   for the arctic atmosphere: ice diatoms, Mar. Biol., 121, 381–387,

752   doi:10.1007/BF00346748, 1994.

754   Levasseur, M., Impact of Arctic meltdown on the microbial cycling of sulphur, Nat.

755   Geosci., 6, 691–700, doi:10.1038/ngeo1910, 2013.

756

757   Lizotte, M., Levasseur, M., Michaud, S., Scarratt, M., Merzouk, A., Gosselin, M.,

758   Pommier, J., Rivkin, R., and Kiene, R.: Macroscale patterns of the biological

759   cycling of dimethylsulfoniopropionate (DMSP) and dimethylsulfide (DMS) in the

760   Northwest Atlantic, Biogeochemistry, 110, 183–200, doi:10.1007/s10533-011-

761   9698-4, 2012.

762

763   Loose, B., McGillis, W.R., and Schlosser, P.: Effects of freezing, growth, and ice cover on

764   gas transport processes in laboratory seawater experiments, Geophys. Res. Lett.,

765   36, L05603, doi:10.1029/2008GL036318, 2009.

766

767   Luce, M., Levasseur, M., Scarrat, M.G., Michaud, S., Royer, S.-J., Kiene, R., Lovejoy,

768   C., Gosselin, M., Poulin, M., Gratton, Y., and Lizotte, M.: Distribution and microbial

769   metabolism of dimethylsulfoniopropionate and dimethylsulfide during the 2007

770   Arctic ice minimum, J. Geophys. Res.-Oceans, 116, C00G06,

771   doi:10.1029/2010JC006914, 2011.

772

773   Malin, G., Wilson, W.H., Bratbak, G., Liss, P.S., and Mann, N.H.: Elevated production of

774   dimethylsulfide resulting from viral infection of cultures of Phaeocystis pouchetii,

775   Limnol. Oceanogr., 43, 1389–1393, doi: 10.1016/S0967-0645(02)00184-4, 1998.

776

777   Martin, J., Tremblay, J. Gagnon, J., Tremblay, G., Lapoussière, A., Jose, C., Poulin, M.,

778   Gosselin, M., Gratton, Y., and Michel, C.: Prevalence, structure and properties of

779   subsurface chlorophyll maxima in Canadian Arctic waters, Mar. Ecol. Prog. Ser.,

780   412, 69–84, doi:10.3354/meps08666, 2010.

781

782   Matrai, P., and Vernet, M.: Dynamics of the vernal bloom in the marginal ice zone of the

783   Barents Sea: Dimethyl sulfide and dimethylsulfoniopropionate budgets, J. Geophys.

784   Res.-Oceans, 102, 22965-22929, doi:10.1029/96JC03870, 1997.

785

786   Michel, C., Ingram, R. G., and Harris, L. R.: Variability in oceanographic and ecological

787   processes in the Canadian Arctic Archipelago, Prog. Oceanogr., 71, 379–401,

788   doi:10.1016/j.pocean.2006.09.006, 2006.

789

790   Motard‑Côté, J., Levasseur, M., Scarratt, M.G., Michaud, S., Gratton, Y., Rivkin, R.B.,

791   Keats, K., Gosselin, M., Tremblay, J.-É., and Kiene, R.P.: Distribution and

792   metabolism of dimethylsulfoniopropionate (DMSP) and phylogenetic affiliation of

793   DMSP‑assimilating bacteria in northern Baffin Bay/Lancaster Sound, J. Geophys.

794   Res-Oceans, 117, C00G11, doi:10.1029/2011JC007330, 2012.

795

796   Mungall, E., Croft, B., Lizotte, M., Thomas, J., Murphy, J., Levasseur, M., Martin, R.,

797   Wentzell, J., Liggio, J., and Abbatt, J.: Dimethyl sulfide in the summertime Arctic

798   atmosphere: measurements and source sensitivity simulations, Atmos. Chem. Phys.,

799   16, 6665–6680, doi:10.5194/acp-16-6665-2016, 2016.

800

801   Nightingale, P.D., Malin, G., and Law, C.S.: In situ evaluation of air‑sea gas exchange

802   parameterizations using novel conservative and volatile tracers, Global

803   Biogeochem. Cy., 14, 373-387, doi:10.1029/1999GB900091, 2000.

804

805   Pinckney, J., Papa, R., and Zingmark, R.: Comparison of high-performance liquid

806   chromatographic, spectrophotometric, and fluorometric methods for determining

807   chlorophyll a concentrations in estaurine sediments, Journal of Microbiol. Meth.,

808   19, 59–66, doi:10.1016/0167-7012(94)90026-4, 1994.

809

810   Quinn, P.K., and Bates, T.S.: The case against climate regulation via oceanic

811   phytoplankton sulphur emissions, Nature, 480, 51-56, doi: 10.1038/nature10580,

812   2011.

813

814   Saltzman, E.S., King, D.B., Holmen, K., and Leck, C.: Experimental determination of the

815   diffusion coefficient of dimethylsulfide in water, J. Geophys. Res., 98, 16481–

816   16486, doi:10.1029/93JC01858, 1993.

817

818   Scarratt, M., Levasseur, M., Michaud, S., and Roy, S.: DMSP and DMS in the Northwest

819   Atlantic: Late-summer distributions, production rates and sea-air fluxes, Aquat.

820   Sci., 69, 292–304, doi:10.1007/s00027-007-0886-1, 2007.

821

822   Simó, R., and Pedrós-Alió, C.: Role of vertical mixing in controlling the oceanic

823   production of dimethyl sulphide, Nature, 402, 396–399, doi:10.1038/46516, 1999.

824

825   Simó, R.: Production of atmospheric sulfur by oceanic plankton: Biogeochemical,

826   ecological and evolutionary links, *Trends Ecol. Evol.*, **16**, 287–294,

827   doi:10.1016/S0169-5347(01)02152-8, 2001.

828

829   Smith, W., Marra, J., Hiscock, M., and Barber, R.: The seasonal cycle of phytoplankton

830   biomass and primary productivity in the Ross Sea, Antarctica, Deep-Sea Res. Pt.

831   II., 47, 3119–3140, doi:10.1016/S0967-0645(00)00061-8, 2000.

832

833 Stefels, J., Steinke, M., Turner, S., Malin, G., and Belviso, S.: Environmental constraints

834   on the production and removal of the climatically active gas dimethylsulphide

835   (DMS) and implications for ecosystem modelling, Biogeochemistry, 83, 245–275,

836   doi:10.1007/s10533-007-9091-5, 2007.

837

838 Sunda, W., Kieber, D.J., Kiene, R.P., and Huntsman, S.: An antioxidant function for

839   DMSP and DMS in marine algae, Nature, 418, 317–20, doi:10.1038/nature00851,

840   2002.

841

842 Taylor, R. L., Semeniuk, D. M., Payne, C. D., Zhou, J., Tremblay, J., Cullen, J. T., and

843   Maldonado, M. T.: Colimitation by light, nitrate, and iron in the Beaufort Sea in

844   late summer, J. Geophys. Res.-Oceans, 118, 3260–3277, doi:10.1002/jgrc.20244,

845   2013.

846

847 Tortell, P.D., Dissolved gas measurements in oceanic waters made by membrane inlet

848   mass spectrometry, Limnol. Oceanogr.-Meth., 3, 24-37, doi:

849   10.4319/lom.2005.3.24, 2005.

850

851 Tortell, P. D., Guéguen, C., Long, M. C., Payne, C. D., Lee, P., and DiTullio, G. R.:

852   Spatial variability and temporal dynamics of surface water pCO2, ΔO2/Ar and

853   dimethylsulfide in the Ross Sea, Antarctica, Deep-Sea Res. Pt. I., 58, 241–259,

854   doi:10.1016/j.dsr.2010.12.006, 2011.

855

856   Tremblay, J.E., Michel, C., Hobson, K.A., Gosselin, M., and Price, N.: Bloom dynamics

857   in early opening waters of the Arctic Ocean, Limnol. Oceanogr. 51, pp.900-912.

858   doi: 10.4319/lo.2006.51.2.0900, 2006.

859

860   Tremblay, J., Bélanger, S., and Barber, D.G.: Climate forcing multiplies biological

861   productivity in the coastal Arctic Ocean, Geophys. Res. Lett., 38,

862   doi:10.1029/2011GL048825, 2011.

863

864   Vallina, S.M., and Simó, R.: Strong relationship between DMS and the solar radiation

865   dose over the surface ocean, Science, 315, 506-8. doi: 10.1126/science.1133680

866

867   Welschmeyer, N.A., Fluorometric analysis of chlorophyll a in the presence of chlorophyll

868   b and pheopigments, Limnol. Oceanogr., 39, 1985-1992,

869   doi:10.4319/lo.1994.39.8.1985, 1994.

870

871   Wolfe, G.V., Strom, S.L., Holmes, J.L., Radzio, T. and Olson, M.B.:

872   Dimethylsulfoniopropionate cleavage by marine phytoplankton in response to

873   mechanical, chemical, or dark stress. J. Phycol., 38, 948-960. doi:10.1046/j.1529-

874   8817.2002.t01-1-01100.x, 2002.

875

876   Woodhouse, M.T, Carslaw, K.S., Mann, G.W., Vallina, S.M., Vogt, M., Halloran, P.R.,

877   and Boucher, O.: Low sensitivity of cloud condensation nuclei to changes in the

878   sea-air flux of dimethyl-sulphide, Atmos. Chem. Phys., 10, 7545–7559,

879   doi:10.5194/acp-10-7545-2010, 2010.

880

881   Zubkov, M.V, Fuchs, B., Archer, S., Kiene, R., Amann, R., and Burkill, P.: Linking the

882   composition of bacterioplankton to rapid turnover of dissolved

883   dimethylsulphoniopropionate in an algal bloom in the North Sea, Environ.

884   Microbiol., 3, 304–311, doi:10.1046/j.1462-2920.2001.00196.x, 200

885

886

887

888

889

890

891

892

893

894

895

896

897

898

899

900

901

902

903

904

905

    Tables

Pigment	Associated Taxa
Chlorophyll c$_3$	Haptophytes
Peridinin	Dinoflagellates
19'-butanoyloxyfucoxanthin	Haptophyte
Fucoxanthin	Diatoms, Haptophytes
19'-hexanoyloxyfucoxanthin	Haptophytes, Dinoflagellates
Diadinoxanthin	Haptophytes, Dinoflagellates,
Violaxanthin	Diatoms Dinoflagellates
Zeaxanthin	Dinoflagellates

908

909

910   **Table 1. HPLC marker pigments and their associated phytoplankton taxa. Adapted**

911   **from Coupel et al. (2015) .**

912

913

914

915

916

917

Station	Lat(N)	Lon(E)	MLD(m)	% Ice Cover	chla (ug L⁻¹)	DMS/chla (nmol µg⁻¹)	DMSP/chla (nmol µg⁻¹)	Perid/chla	19'ButFuc/chla	Fuc/chla	19'HexFuc/chla	Diadino/chla
K1	56.12	-53.37	18.4	*nd*	0.51	6.6	*nd*	0.043	0.077	0.184	0.156	0.056
LS2	60.45	-56.55	41.4	*nd*	0.59	3.4	*nd*	0.051	0.012	0.277	0.025	0.024
BB3	71.41	-68.59	8.2	19.7	0.12	*bdl*	129.4	0.049	0.011	0.278	0.051	0.087
BB2	72.75	-67.00	10.3	*nd*	0.19	21.7	93.3	0.050	0.015	0.312	0.089	0.072
CAA1	74.52	-80.56	32.1	*nd*	0.56	6.9	52.3	0.015	0.018	0.239	0.023	0.042
CAA5	74.12	-91.49	5.3	6.61	0.16	*bdl*	114.7	0.078	0.017	0.326	0.020	0.051
CAA6	74.75	-97.47	6.1	16.43	0.21	10.6	181.7	0.054	0.021	0.401	0.015	0.058
CAA7	73.66	-96.53	2.1	13.3	0.13	15.6	81.3	0.109	0.066	0.335	0.057	0.146
VS	69.16	-100.69	8.4	8.23	0.18	10.6	*nd*	0.029	0.020	0.309	0.032	0.037

Table 2. Mixed layer depth (MLD), ice cover, HPLC pigment measurements (ratios of selected marker pigments to chl a), DMS (MIMS) and DMSP (OSSCAR) measurements. Perid = peridinin, 19'ButFuc = 19'-butanoyloxyfucoxanthin, Fuc = Fucoxanthin, 19'HexFuc = 19'-hexanoyloxyfucoxanthin, Diadino = Diadinoxanthin. *nd*= no data. *bdl* = below detection limit.

940

Station	Diatom	Dinoflag.	Chloro.	Prasino	Crypto.	C-P	c3-Flag.	Hapto-7
K1	37	14	0	17	4	9	1	16
LS2	39	19	0	23	1	3	7	8
BB3	48	15	4	14	8	1	5	5
BB2	44	16	11	14	4	2	1	8
CAA1	47	4	0	39	2	2	4	2
CAA5	50	19	1	10	3	2	14	1
CAA6	52	16	1	8	3	2	17	1
CAA7	46	11	4	17	8	8	0	5
VS	67	8	0	11	3	3	6	3

941

942 **Table 3.** CHEMTAX-derived phytoplankton assemblage estimates (numbers given are

943 percent of total chl a) for sampled stations. Diat. = diatoms; Dinoflag = Dinoflagellates;

944 Chloro. = Chlorophytes; Prasino = Prasinophyte (types 2 and 3); Crypto. = Cryptophytes

945 Chryso-Pelago =Chrysophytes/Pelagophytes; c3-flag. = c3-Flagellates; Hapto-7 =

946 Haptophyte type 7. Due to the presence of unidentified phytoplankton taxa, not all

947 assemblage estimates sum to 100%.

948

949

Variable	DMS Correlation Coefficient	DMSP Correlation Coefficient
$\Delta O_2/Ar$	0.22	0.33
Salinity	0.35	0.34
SST	0.29	0.14
Fluorescence	0.32	0.66
pCO_2	0.16	0.12
Ice Cover	-0.26	-0.34

950

951 **Table 4.** Pearson correlation coefficients relating DMS measurements made by MIMS

952 and DMSP measurements made by OSSCAR to other oceanographic variables. Only

953 correlations significant at the $p < 0.05$ level are shown. $\Delta O_2/Ar$ ratios were obtained using

954 MIMS.

Author	Year	Month	Region	DMS (nM)	DMSP (nM)	Assemblage characteristics
Bouillon et al. 2002	1998	April-June	North Water	0.04-6.7	0.9-53	Diatom dominated assemblage
Matrai et al. 1997	1993	May	Barents Sea	2.8 - 25.3	6-27	Diatom-dominated and *Phaeocystis*-dominated stations
Lizotte et al. 2012	2003	May-October	Northwest Atlantic	0.1-12	4-101	Nanoflagellate dominated in all seasons
Gali et al. 2010	2007	July	Greenland Sea	0.1 - 18.3	1.4 - 163.6	Haptophyte (*Phaeocystis*) dominance
Leck et al. 1996	1991	August-October	Greenland Sea	0.04 - 12	--	Not described
Motard-Côté et al. 2012	2008	September	Baffin Bay North Water	0.4-5.2	5–70	
Scarratt et al. 2007	1999	September	Northwest Atlantic	0.2-4.7	0-203	Mixed assemblage
Luce et al. 2011	2007	October-November	High Arctic	0.05-0.8	2- 39	Flagellate-dominated except for diatom-dominated in Baffin Bay

Table 5. Compilation of published Arctic and Subarctic Atlantic DMS/P data from the summer and fall months, focusing on observations from the Western Hemisphere.

Figures:
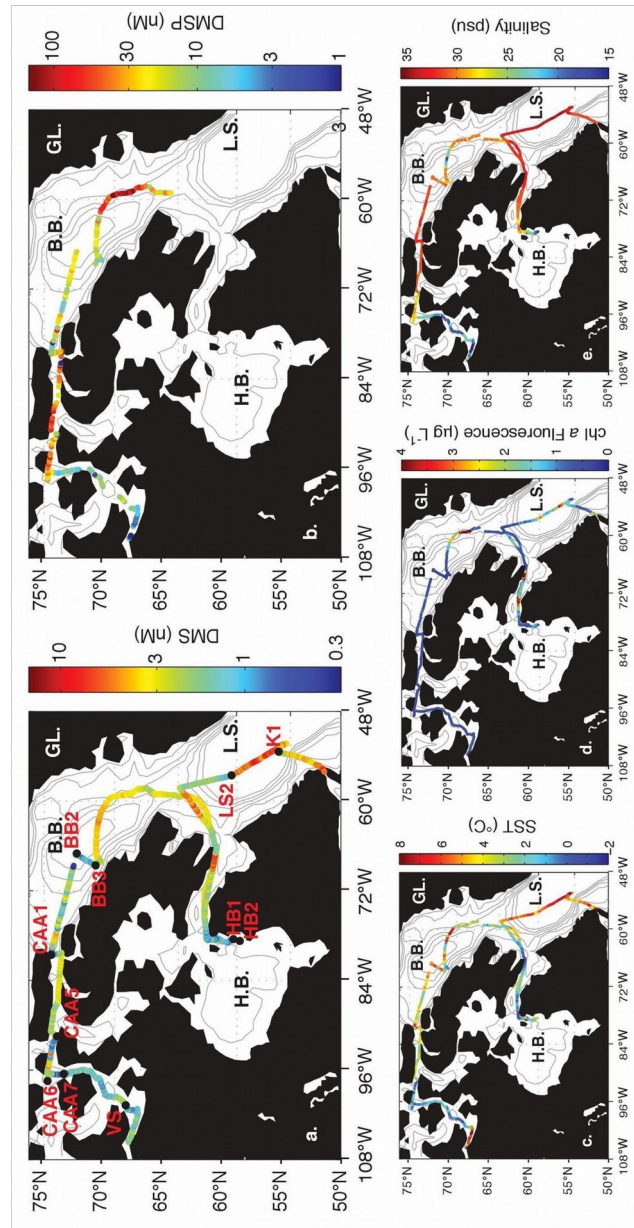
Figure 1. Spatial distribution of DMS, DMSP and hydrographic variables. GL. =

Greenland, B.B. = Baffin Bay, L.S = Labrador Sea, H.B. = Hudson Bay, C.A.A. =

Canadian Arctic Archipelago.

992
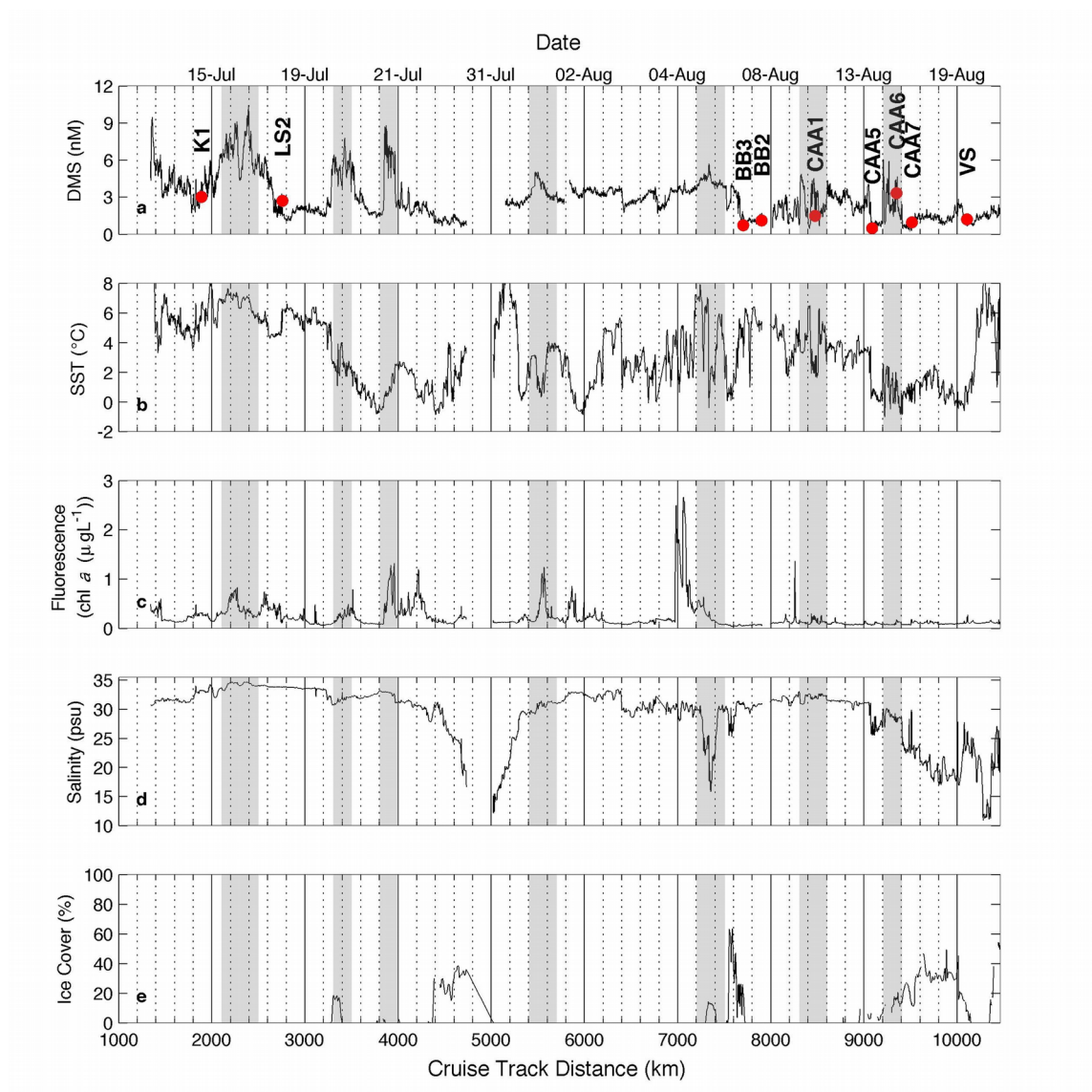
993 **Figure 2.** Distribution of DMS and hydrographic variables along our cruise track. Grey

994 shaded areas denote regions of sharp increases in DMS. Labeled red dots indicate

995 sampling stations (see Table 2).

996
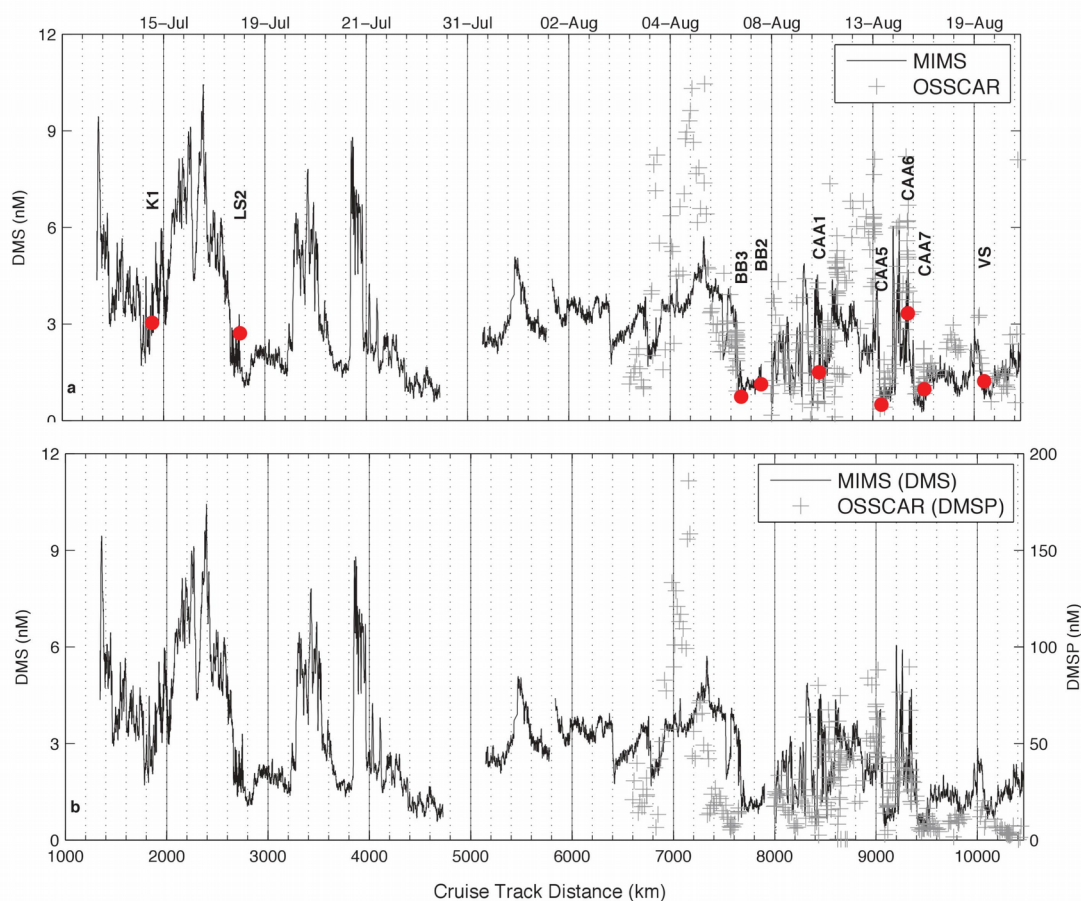
998   **Figure 3.** Distribution of DMS and DMSP along the cruise track. Panel (a) shows DMS

999   measurements made by MIMS and OSSCAR.   Note that a small fraction (less than

1000   0.5%) of measurements made by OSSCAR were above 12 nM. Panel (b) shows MIMS

1001   data with OSSCAR DMSP measurements superimposed on a different y scale (right hand

1002   side). Labeled red dots indicate DMS concentrations measured at discrete sampling

1003   stations (see Table 2).

1004

1005

1006

1007

1008

1009

1010

1011

1012

1013

1014

1015

1016

1017

1018

1019

1020

1021   Figure 4. Distribution of DMS, wind speed, sea ice cover and sea-air DMS flux along the

1022   cruise track.

1023

1024

1025

1026

1027

1028

1029

1030

1031

1032

1033

1034

1035

1036

1037

1038

1039

1040

1041

1042

1043
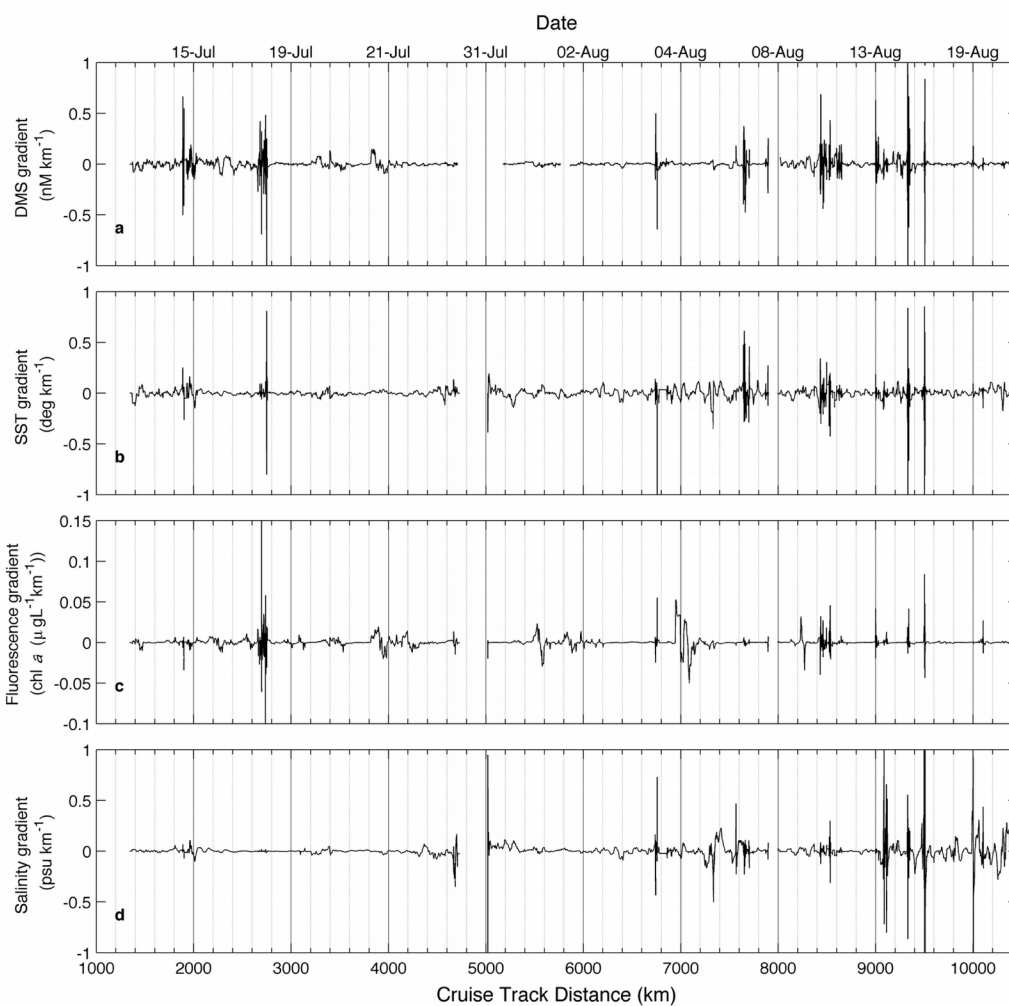
1044   **Figure 5.** Spatial gradients in DMS (measured with MIMS) and hydrographic variables,

1045   calculated from a neighbourhood of 100 data points (~25km).

1046

1047

1048

1049

1050

1051

1052

1053

1054

1055

1056

1057

1058

1059

1060

1061

1062

1063

1064

1065

1066
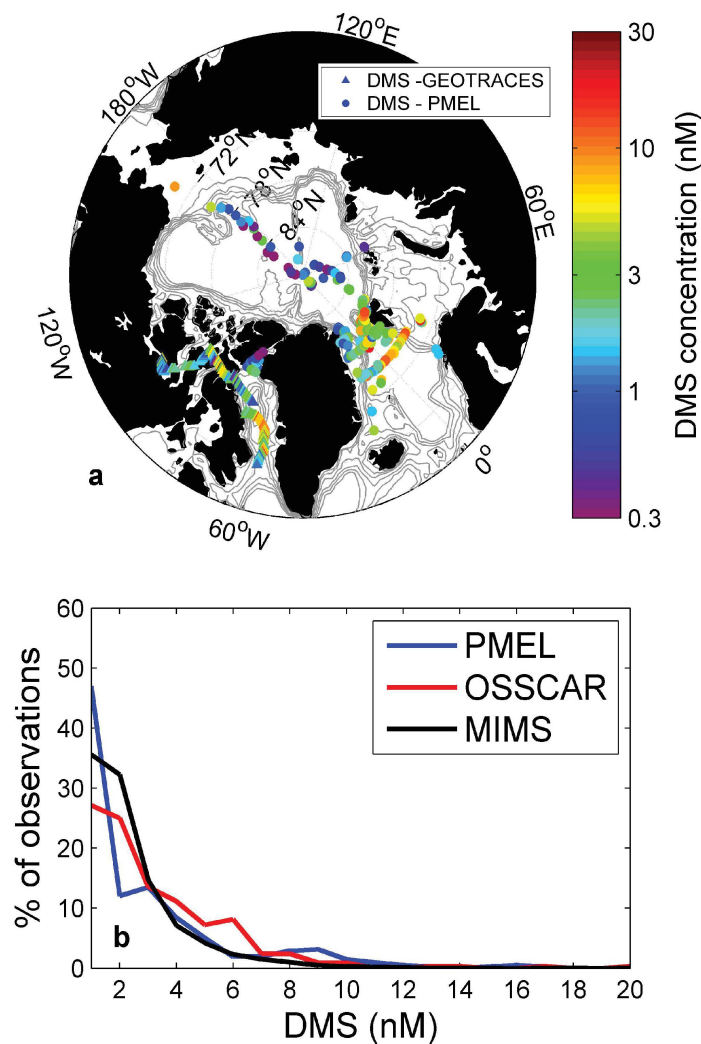
Figure 6. Comparison of OSSCAR- and MIMS-measured DMS from this study with existing summertime data in the PMEL database. Panel (a) shows the geographic distribution of DMS measurements in the PMEL database and those obtained by this study (using OSSCAR), while panel b) shows a histogram of DMS concentrations in three datasets – the MIMS dataset (33,250 data points) the OSSCAR dataset (344 points) , and the PMEL dataset. (415 points).